Journal of Nuclear Medicine, published on February 3, 2022 as doi:10.2967/jnumed.121.263254

First-in-human evaluation of ^{18}F-SMBT-1, a novel ^{18}F-labeled MAO-B PET tracer for imaging reactive astrogliosis

Victor L Villemagne,[1,2] Ryuichi Harada,[3,4] Vincent Doré,[2,5] Shozo Furumoto,[6] Rachel Mulligan,[2] Yukitsuka Kudo,[4] Samantha Burnham,[5] Natasha Krishnadas,[2] Svetlana Bozinovski,[2] Kun Huang,[2] Brian J Lopresti,[7] Kazuhiko Yanai,[3] Christopher C Rowe,[2,8,9] and Nobuyuki Okamura.[10]

1. *Department of Psychiatry, University of Pittsburgh, Pittsburgh, PA, USA*
2. *Department of Molecular Imaging & Therapy, Austin Health, Melbourne, Australia*
3. *Department of Pharmacology, Tohoku University School of Medicine, Sendai, Japan*
4. *Institute of Development of Aging and Cancer, Tohoku University, Sendai, Japan*
5. *CSIRO Health and Biosecurity Flagship: The Australian e-Health Research Centre, Melbourne, Australia*
6. *Cyclotron and Radioisotope Center, Tohoku University, Sendai, Japan*
7. *Department of Radiology, University of Pittsburgh, Pittsburgh, PA, USA*
8. *The Florey Institute of Neuroscience and Mental Health, The University of Melboourne, Melbourne, Australia*
9. *The Australian Dementia Network*
10. *Division of Pharmacology, Faculty of Medicine, Tohoku Medical and Pharmaceutical University, Sendai, Japan*

Corresponding author: Victor L Villemagne
Address: Department of Psychiatry, University of Pittsburgh School of Medicine, 3811 O'Hara St. Pittsburgh PA, 15213, USA.
Tel: +1 412-246-6010
Email: victor.villemagne@pitt.edu

Key Words: Reactive astrogliosis, MAO-B, Alzheimer's disease, amyloid, brain imaging

Running Title: *In vivo imaging of reactive astrogliosis*

Disclosure: Yukitsuka Kudo and Nobuyuki Okamura own stock in Clino Ltd licensing SMBT-1. Ryuichi Harada, Shozo Furumoto, Yukitsuka Kudo, and Nobuyuki Okamura have a patent pending for the technology described in this article. No other potential conflicts of interest relevant to this article exist.

ABSTRACT

Background: Reactive gliosis changes, characterized by reactive astrocytes and activated microglia, contribute greatly to neurodegeneration throughout the course of Alzheimer's disease (AD). Reactive astrocytes overexpress monoamine oxidase-B (MAO-B). We characterized the clinical performance of ^{18}F-SMBT-1, a novel MAO-B PET tracer as a potential surrogate marker of reactive astrogliosis.

Methods: Seventy-seven participants –53 controls (CN), 7 mild cognitively impaired (MCI), 7 AD patients, and 10 young controls (YCN)– were recruited for the different aspects of the study. Older participants underwent 3D-MPRAGE MRI and Aβ, tau, and ^{18}F-SMBT-1 imaging with PET. To ascertain ^{18}F-SMBT-1 selectivity to MAO-B, 9 participants underwent two ^{18}F-SMBT-1 scans, before and after receiving 5mg selegiline twice daily for 5 days. To compare selectivity, ^{18}F-THK5351 studies were also conducted before and after selegiline. Aβ burden was expressed in Centiloids. ^{18}F-SMBT-1 outcomes were expressed as standard uptake value, as well as tissue ratios and binding parameters using the subcortical white matter as reference region.

Results: ^{18}F-SMBT-1 showed robust entry into the brain and reversible binding kinetics, with high tracer retention in basal ganglia, intermediate in cortical regions, and lowest in cerebellum and white matter which tightly follows the known regional brain distribution of MAO-B (R^2=0.84). More than 85% of ^{18}F-SMBT-1 signal was blocked by selegiline across the brain and, in contrast to ^{18}F-THK5351, no residual cortical activity was observed after the selegiline regimen, indicating high selectivity for MAO-B and low non-specific binding. ^{18}F-SMBT-1 also captured the known MAO-B increases with age, with an annual rate of change (~2.6%/yr), similar to the in vitro rates of change (~1.9%/yr). Quantitative and semiquantitative measures of ^{18}F-SMBT-1 binding were highly associated (R^2>0.94), suggesting a simplified tissue ratio approach could be used to generate outcome measures.

Conclusions: ^{18}F-SMBT-1 is a highly selective MAO-B tracer, with low non-specific binding, high entry into the brain and displaying reversible kinetics. Moreover, ^{18}F-SMBT-1 brain distribution matches the reported in vitro distribution and captures the known MAO-B increases with age, suggesting ^{18}F-SMBT-1 can potentially be used as a surrogate marker of reactive astrogliosis. Further validation of these findings with ^{18}F-SMBT-1 will require examination of a much larger series, including participants with MCI and AD.

INTRODUCTION

The neuropathological hallmarks of Alzheimer's disease (AD), neurofibrillary tangles of tau protein and amyloid-β (Aβ) plaques, are accompanied by reactive gliosis, cellular degeneration, and diffuse synaptic and neuronal loss. (*1*)

In recent years, there has been an increased interest in the study of astrocytes. (*2*) Astrocytes are the most abundant glial cells in the brain and are involved in several functions critical for the normal functioning and preservation of brain homeostasis (*3,4*) such as synaptic plasticity and formation of memory, (*5,6*) regulation of gamma aminobutyric acid and glutamatergic neurotransmission (*7-9*), regulation of cerebral blood flow (*10,11*) contribute to both Aβ production, (*12*) and Aβ clearance. (*13*) Astrocytes are also essential components of the neuroglial vascular unit, where they play a key neuroprotective role in cerebrovascular disease. (*10,11*) Astrocytes do not constitute a homogenous population, and have been morphologically classified into protoplasmic, fibrous and interlaminar, or by their state: resting and/or activated. (*14*) While reactive astrocytes have also been classified as neurotoxic (A1), characterized by the expression of complement fraction 3 and neuroprotective (A2) expressing the S100A10 protein, (*15,16*) reactive astrogliosis constitute a much more complex spectrum of toxic and protective pathways, (*2,17*) playing a crucial role in the pathophysiology of AD. (*9,18*) Astrogliosis is an early neuroinflammatory event in several neurodegenerative conditions (*19*) such as Alzheimer's disease (AD) (*7,9,18*), making it a target for the in vivo assessment of neuroinflammatory processes and their potential synergistic or independent contribution to the development of AD dementia. In AD, reactive astrogliosis and microgliosis have been observed around both dense-core Aβ plaques and neurofibrillary tangles, and they are believed to contribute greatly to neurodegeneration throughout the course of the disease (*18,20*). In contrast to microgliosis which is not detected by imaging at early disease stages, (*21*) reactive astrogliosis occurs early, (*22*) making it a particularly attractive target for understanding the contribution of astrogliosis to AD pathogenesis and the development of dementia and, as such, a potential therapeutic target for AD (*23*).

Reactive astrocytes overexpress monoamine oxidase B (MAO-B), (*24*) and molecular neuroimaging studies have employed MAO-B tracers such as ^{11}C-L-deprenyl-D2 (^{11}C-DED) as surrogate markers of astrogliosis. (*22,25-28*) Some of these studies have shown that reactive astrogliosis is observed at the prodromal stages in both sporadic and familial AD. (*22,25*) Historically, ^{11}C-DED has been used as a surrogate PET tracer for reactive astrogliosis, however several issues limit the use of ^{11}C-DED such as difficulty to quantify due to its irreversible kinetics, the existence of radiolabeled

metabolites that can cross the blood-brain barrier (BBB) and bind to monoamine transporters, poor image quality and low selectivity for MAO-B. (*29*) More recently another MAO-B tracer, ^{11}C-SL25.1188 with more favorable tracer kinetics than ^{11}C-DED was developed. (*30,31*) ^{11}C-BU99008 a tracer for the imidazoline 2 binding sites (I2BS) has also been proposed as a surrogate marker of astrogliosis. (*32-35*) Unfortunately, like ^{11}C-DED, these tracers are labeled with 20-min half-life C-11 preventing widespread clinical or research applications.

Recently, an analog of the PET radiotracer ^{18}F-THK5351, which was developed as a putative tau imaging radiotracer (*36*) but was later shown to have significant MAO-B binding, (*37,38*) has been identified to be highly selective for MAO-B. (*39*) The preclinical assessment showed [^{18}F](*S*)-(2-methylpyrid-5-yl)-6-[(3-fluoro-2-hydroxy)propoxy]quinoline (^{18}F-SMBT-1), binds with high affinity (K_D=3.5 nM) and selectivity to MAO-B in human brain homogenates (*39*). Comparison of in vitro ^{18}F-SMBT-1 binding against MAO-B regional activity expressed as relative luminescence showed SMBT-1 binding to be highly correlated with the regional activity of MAO-B in the brain (*39*). Autoradiography studies showed significantly higher specific binding in the frontal cortex of an AD patient compared to control (*39*). Specific binding of ^{18}F-SMBT-1 was completely displaced after incubation with 1µM of the selective MAO-B inhibitor lazabemide, (*39*) showing high selectivity and low non-specific binding. Receptor binding screen assays showed no significant SMBT-1 binding to 60 common neurotransmitter receptors, ion channels, and transporters. (*39*) Radiation exposure was extrapolated to be 21.3 µSv/MBq for women and 12.2 µSv/MBq for men (*39*). Toxicity studies of SMBT-1 in animals, including acute pharmacology and toxicity at doses 1,000-10,000 times higher than those expected in a PET study, demonstrated no toxic effects related to the drug treatment.

The aim of this first-in-human study was to characterize ^{18}F-SMBT-1 binding, assessing its relation to age, regional brain distribution and selectivity for MAO-B. We also examined ^{18}F-SMBT-1 tracer kinetics and explored potential quantification approaches.

MATERIALS AND METHODS

Participants

A total of 77 non-smoking participants –53 controls (CN), 7 mild cognitively impaired (MCI), 7 AD patients, and 10 young controls (YCN)– were recruited for the different aspects of the study. All participants were screened for unstable medical and/or psychiatric disease and concomitant medication. Participants with known use of antidepressants, cold and flu tablets, opiate or opioid agonist medication

were excluded from the study due to the possibility of interactions with selegiline. For participants with a recognized memory impairment, this information was collected from a next of kin or caregiver. The study protocol was approved by the Austin Health Human Research Ethics Committee, and all participants gave written informed consent.

PET Image Acquisition

PET scans were acquired on one of two scanners, a Philips TF64 PET/CT or a Siemens Biograph mCT. A low dose CT was obtained for attenuation correction. Partial volume correction was not performed in any of the studies.

^{18}F-SMBT-1 imaging. ^{18}F-SMBT-1 was synthesized in-house in the Department of Molecular Imaging & Therapy, Austin Health, VIC, Australia using an ORA Neptis radiosynthesiser. ^{18}F-SMBT-1 synthesis is detailed in Supplementary Materials. Sixty-nine adults (10 YCN, 49 older CN, 6 MCI and 4 AD patients) participated in the assessment of ^{18}F-SMBT-1. All participants were administered 186±6 MBq of ^{18}F-SMBT-1 (range 177-194 MBq). The average administered mass of ^{18}F-SMBT-1 was 1.0±0.8 micrograms (range 0.10– 2.60 micrograms). Of the 69, 10 non-demented participants (4 controls and 6 MCI) underwent a 90 min dynamic scanning after intravenous bolus injection of ^{18}F-SMBT-1. The remaining 59 participants (10 YCN, 45 controls and 4 AD patients) underwent a 20-minute emission scan (4 x 5 min) starting at 60 minutes post injection of ^{18}F-SMBT-1. A second ^{18}F-SMBT-1 PET scan was acquired in 9 participants (5 controls and 4 AD patients) after completion of a 5-day regimen of oral selegiline.

Aβ Imaging. All 67 older adults underwent Aβ PET imaging with either ^{18}F-Flutemetamol (FLUTE, n=3), ^{18}F-Florbetapir (FBP, n=2) or ^{18}F-NAV4694 (NAV, n=62) to ascertain Aβ status. NAV and FBP were synthesized in-house in the Department of Molecular Imaging & Therapy, Austin Health, VIC, Australia, as previously reported. (*40-42*) FLUTE was manufactured by Cyclotek Pty Ltd, (www.cyclotek.com). The NAV and FBP PET scan acquisition consisted of a 20 minute (4 x 5 min) dynamic scans acquired at 50 minutes after an intravenous bolus injection of 185 MBq (±10%) of NAV or FBP. Similarly, the participants who received FLUTE also underwent a 20-minute (4 x 5 min) PET acquisition starting at 90 minutes after injection of 185 MBq (±10%) of FLUTE. All Aβ imaging results were expressed in Centiloids (CL) (*40,41,43,44*).

Tau Imaging. Nine older adults enrolled in the selegiline assessments with ^{18}F-SMBT-1 also underwent tau imaging with either ^{18}F-MK6240 (n=7) or ^{18}F-PI2620 (n=2). Both tau imaging tracers were synthesized in-house in the Department of Molecular Imaging & Therapy, Austin Health, VIC, Australia,

as previously reported. (*45*) The ^{18}F-MK6240 PET scan acquisition consisted of a 20 minute (4 x 5 min) dynamic scans acquired at 90 minutes after an intravenous bolus injection of 185 MBq (±10%) of ^{18}F-MK6240. The ^{18}F-PI2620 PET scan acquisition consisted of a 20 minute (4 x 5 min) dynamic scans acquired at 80 minutes after an intravenous bolus injection of 200 MBq (±10%) of ^{18}F-PI2620. All tau imaging results were expressed as standard uptake value ratios (SUVR) using the cerebellar cortex as reference region.

^{18}F-THK5351. Imaging. Eight older adults (4 CN, 1 MCI and 3 AD patients) underwent two ^{18}F-THK5351 PET scans. ^{18}F-THK5351 was synthesized in-house in the Department of Molecular Imaging & Therapy, Austin Health, VIC, Australia, as previously described (*46*). Participants received an intravenous bolus injection of 185 MBq (±10%) of ^{18}F-THK5351 and a 30-minute emission scan (4 x 5 min) was acquired starting at 50 minutes post injection. A second ^{18}F-THK5351 PET scan was acquired after completion of a 5-day regimen of oral selegiline.

MRI Acquisition

Participants were also asked to undergo a structural magnetic resonance imaging (MRI) on a Siemens 3-T TIM Trio scanner (Siemens Medical Solutions) to obtain high-resolution T1-weighted anatomical magnetization prepared rapid gradient echo (MPRAGE) sequences.

Image Analysis

Aβ and tau PET scans were spatially normalized using CapAIBL. (*44*) The standard Centiloid (CL) method was applied to determine Aβ burden. (*43*) A CL value >20 was selected to determine a high Aβ (Aβ+) scan (*47*). A 1.19 SUVR in the temporal composite region (*48*) was used to discriminate between high tau (T+) and low tau (T-). ^{18}F-THK5351 scans were spatially normalized using CapAIBL and expressed as standard uptake values (SUV). ^{18}F-SMBT-1 PET images were also spatially normalized using CapAIBL. ^{18}F-SMBT-1 PET volumes of interest were sampled to assess tracer selectivity, regional distribution, effect of age, and kinetic analysis. SUV values for the selegiline studies were estimated in four composite grey matter volumes of interest: neocortex (NCTX, comprising frontal, superior parietal, lateral temporal and lateral occipital, anterior and posterior cingulate gyri and precuneus), mesial temporal lobe (MTL, comprising hippocampus, entorhinal cortex, parahippocampus and amygdala), basal ganglia (BG, comprising caudate, putamen, globus pallidus and thalamus) and cerebellar cortex. Several brain regions were evaluated as potential reference tissue, before generating semiquantitative tissue ratios/SUV ratios (SUVR) and graphical analysis of the data. Kinetic analysis was performed using PMOD (PMOD Technologies, Zurich, Switzerland, www.pmod.com).

Assessing tracer selectivity using Selegiline

Seventeen volunteers participated in the selegiline study. Following a baseline ^{18}F-THK5351 or ^{18}F-SMBT-1 PET scan, participants were supplied with the selegiline medication and were instructed to follow a 5-day regimen of the oral tablets at the standard therapeutic dose of 10 mg daily (5 mg at breakfast and 5 mg at lunch). At the completion of the regimen participants were invited back for a repeat PET scan.

Statistical analyses

All statistical analyses were performed with JMP Pro 15 for Macintosh (JMP® Pro Version 15, SAS Institute Inc., Cary, NC, 1989-2019). Data are presented as mean ± standard deviation (SD) unless otherwise stated. Statistical evaluations between groups were performed using paired or unpaired Student's t-tests. Effect size was measured with Cohen's d. Correlations were assessed by Spearman and Pearson correlation coefficient. Changes in tracer retention between pre- and post-selegiline THK studies was expressed as percentage reduction from baseline (Δ%). Significance was set at $p<0.05$, uncorrected for multiple comparisons.

RESULTS

No significant changes in vital signs, nor immediate or delayed adverse events related to the study drug were observed or reported by any of the participants during or following the ^{18}F-SMBT-1 scan.

Tracer Selectivity Studies

The irreversible MAO-B inhibitor was used to evaluate the selectivity of ^{18}F-SMBT. All participants received an Aβ and tau imaging scan, in addition to the 2 SMBT-1 scans before and after selegiline. The same study was repeated with a different cohort of participants using ^{18}F-THK5351 to assess the validity of the selegiline regimen.

Table 1 shows the demographics of both groups. Tracer selectivity was assessed in 17 participants, 8 of them (4 CN, 3 Aβ+AD, and 1 Aβ+MCI) underwent assessment with ^{18}F-THK5351, while 9 (5 controls and 4 Aβ+AD) underwent assessment with ^{18}F-SMBT-1.

For the selectivity study with ^{18}F-THK5351, 8 participants underwent Aβ imaging and two ^{18}F-THK5351 PET scans, one at baseline and one after a 5-day regimen of 5 mg oral selegiline twice daily.

Figure 1A shows on the top row Aβ imaging studies expressed in CL in a cognitively unimpaired control (CN) -performed with ^{18}F-flutemetamol- and in an AD patient -performed with ^{18}F-NAV4694-, the middle row shows baseline ^{18}F-THK5351 PET images of the same individuals expressed in Standard Uptake Value (SUV) images before and after (bottom row) the selegiline regimen indicating a variable degree of blockade of the ^{18}F-THK5351. Given that there is significant reduction in tracer retention in the cerebellar cortex, usually used as reference region, all images are displayed in SUV units. Importantly, there is residual neocortical signal in the follow-up scan of the Aβ+ AD patient that is likely attributable to tau (bottom row). Figure 1B shows a variable decrease in baseline ^{18}F-THK5351 signal in neocortex (~63% decrease), mesial temporal lobe (~71% decrease), basal ganglia (~82% decrease) and cerebellar cortex (~54% decrease), although there were no significant differences in the degree of signal reduction between controls and AD.

For the selectivity study with ^{18}F-SMBT-1, 9 participants (5 elderly controls (CN) and 4 Aβ+T+ AD patients) underwent Aβ and tau imaging and two ^{18}F-SMBT-1 PET scans, one at baseline and one after the same 5-day regimen of 5 mg of oral selegiline twice daily. Figure 1C shows on the first two rows Aβ imaging studies with ^{18}F-NAV4694 expressed in CL and tau imaging studies with ^{18}F-MK6240 expressed as SUV ratio (SUVR) using the cerebellar cortex as reference region, in a cognitively unimpaired control (CN) and in an AD patient. The bottom two rows show ^{18}F-SMBT-1 SUV images before and after the selegiline regimen indicating a very high degree of reduction of the ^{18}F-SMBT-1 signal with no residual activity attributable to Aβ or tau. Figure 1D shows a more than 85% decrease in baseline ^{18}F-SMBT-1 signal in neocortex, MTL, BG and cerebellum with the same degree of signal reduction in controls and AD. A more detailed brain regional blockade by selegiline is provided in Table 2.

Regional Brain Distribution of ^{18}F-SMBT-1

We also assessed the in vivo regional brain distribution of ^{18}F-SMBT-1. Figure 2 shows ^{18}F-SMBT-1 SUV at 60-80 min after injection in 44 Aβ- elderly CN, against the reported in vitro ^{11}C-DED ARG regional concentrations (*49*). There was a high correlation (R^2 = 0.84, p=0.0002) between the in vivo regional ^{18}F-SMBT-1 signal and the in vitro concentrations in several regions of the brain.

MAO-B Increases with Age

To further evaluate ^{18}F-SMBT-1, we scanned 10 young controls (YCN, 5F/5M, 31.3±4.0 yo) (Table 3) to assess if ^{18}F-SMBT-1 was able to capture the age-related increases of MAO-B in the frontal lobe as

previously reported by in vitro studies (*50*). ^{18}F-SMBT-1 SUV in the frontal lobe of 10 YCN and 44 Aβ-T- elderly controls (Figure 3A) demonstrated a significant age-related increase in MAO-B (R^2=0.44, p<0.0001). Figure 3B shows coronal, sagittal and transaxial images illustrating the age-related regional increases in ^{18}F-SMBT-1 signal in three females whose age ranged from 31 to 86 yo. (identified by the red circles on Figure 3A).

SMBT-1 Kinetics.

We characterized the in vivo ^{18}F-SMBT-1 kinetics in 10 elderly participants (6 MCI and 4 controls Table 4). Time activity curves revealed ^{18}F-SMBT-1 has robust entry into the brain (SUV= 4-7 at ~3-5 min after injection) and displays reversible kinetics. (Figure 4A) The highest ^{18}F-SMBT-1 retention was observed in the basal ganglia and thalamus, intermediate in the anterior cingulate, gyrus rectus and hippocampus, low in neocortical areas, and lowest in CB and in the Subcortical White Matter (SWM).

Before generating SUVR over time, we compared the SUV in several potential reference regions: CB; Cerebellar White Matter (CbWM); SWM; (*51*) and SWM also including the Corpus Callosum (SWM+CC) (*52*) to be used in a simplified reference tissue model (*53*). The SUVR generated with the SWM as reference region had the highest correlation with the in vitro regional distribution of MAO-B (Table 5) (*49*).

SUVR were shown to approach apparent steady state in high binding areas ~50 min after injection, (Figure 4B) suggesting the possibility of using a simplified ^{18}F-SMBT-1 imaging protocol with SUVR as outcome. ^{18}F-SMBT-1 reversible kinetics was further validated by graphical analysis of the 90 min dynamic scans, using the same regions used for generating SUVR. ^{18}F-SMBT-1 specific binding measures of volume of distribution (V_T) derived from the non-invasive Logan plot (*54*) as well as binding potential non-displaceable (BP_{ND}) estimated using Ichise's multilinear reference tissue model, MRTM (*55*), showed high correlations with late-scan SUVR (R^2 = 0.97 and R^2 = 0.94, for BP_{ND} and V_T, respectively) and also with the known distribution of MAO-B in the human brain (R^2 = 0.78 and R^2 = 0.72, for BP_{ND} and V_T, respectively) (*49*).

DISCUSSION

To the best of our knowledge, ^{18}F-SMBT-1 represents the first available F-18 MAO-B radiotracer to be used in a clinical study. Preclinical evaluation demonstrated ^{18}F-SMBT-1 to have an in vitro binding profile well suited for a MAO-B PET tracer, (*39*) so the study aimed at characterizing ^{18}F-SMBT-1 binding profile in vivo with PET. The study was divided in four main areas or sub-studies. We first assessed ^{18}F-

SMBT-1 selectivity for MAO-B before and after a 5-day regimen of oral selegiline. ^{18}F-SMBT-1 is an analog of the PET radiotracer ^{18}F-THK5351, which was developed as a putative tau imaging radiotracer (*39*) but was later shown to have significant MAO-B binding (*37,38*). Therefore, we compared the ^{18}F-SMBT-1 results with studies performed with ^{18}F-THK5351 under the same selegiline regimen. For these studies, given that there is significant widespread reduction in tracer retention even in regions usually used as internal reference, all images were displayed in SUV units. In the ^{18}F-THK5351 studies, the degree of blockade by selegiline in grey matter areas was variable, ranging from 54% in the cerebellar cortex to >80% in the basal ganglia. Moreover, there was some residual ^{18}F-THK5351 cortical signal in the cortex likely representing ^{18}F-THK5351 binding to tau. In the ^{18}F-SMBT-1 studies, the degree of blockade by selegiline in grey matter areas was >85%, and most importantly, there was no residual cortical signal. There were no significant differences in the degree of signal reduction between controls and AD with either ^{18}F-THK5351 or ^{18}F-SMBT-1. This study also demonstrated the low degree of non-specific binding with ^{18}F-SMBT-1. This is important because it enables ^{18}F-SMBT-1 to accurately detect incipient early cortical changes in MAO-B concentrations as well as small changes over time. The low non-specific binding is also evident in the high contrast images (Figure 1C**)** even at 60-80 min post injection. We then assessed the regional brain distribution of ^{18}F-SMBT-1 and compared the results to in vitro ARG performed with ^{11}C-DED (*49*) showing a high correlation between the two. The competition studies with selegiline and the regional distribution studies indicate ^{18}F-SMBT-1 is a highly selective F-18-labeled MAO-B tracer (*7*).

^{18}F-SMBT-1 was also able to capture the known MAO-B increases with age. The estimated yearly signal increase for ^{18}F-SMBT-1 in the frontal cortex is ~2.5%/yr, similar to the ~1.9%/yr estimates from in vitro studies (*50*).

Finally, we evaluated the tracer kinetic characteristics of ^{18}F-SMBT-1. The time activity curves showed high initial entry into the brain, followed by clearance of the tracer. Slower clearance was observed in areas with very high MAO-B concentrations like the basal ganglia, intermediate in areas with high MAO-B concentrations like the hippocampus and anterior cingulate, and faster in cortical areas with low concentrations of MAO-B such as the neocortical areas. The lowest retention was observed in SWM. The reversible binding kinetics suggested that ^{18}F-SMBT-1 binding could be quantified using graphical analysis (*54,55*) and a simplified reference tissue model (*53*).

Before embarking in the generation of tissue ratios and graphical analysis of the data, we explored several potential reference regions. We correlated the tissue ratios generated with each of them against

the known regional distribution of MAO-B in the brain. $SUVR_{SWM}$ yielded the highest correlation. Moreover, the SWM was the least affected region by selegiline, (Table 2) and one of the least atrophic regions across the AD continuum (*56*). Graphical analysis outcomes, either MTRM or Logan plot, also generated using the SWM as reference region were highly correlated with $SUVR_{SWM}$ and with the in vitro brain distribution of MAO-B. The small number of MCI and AD patients precludes drawing any conclusion regarding group differences in the SMBT-1 signal. A larger sample size of MCI and AD patients, with their corresponding Aβ and tau status, will be required to examine if ^{18}F-SMBT-1 can capture the reported increases in MAO-B in AD.

While most of the recently developed specific neuroimaging and biofluid markers of disease have focused on the pathological hallmarks of AD, such as Aβ plaques and tau tangles, the most prevalent markers identified in Genome-wide association studies of AD are related to neuroinflammation (*57*). The introduction of biomarker-based approaches for the identification of brain pathology has informed new strategies for the design of preventative clinical trials aimed at preventing the onset of cognitive impairment and dementia. Markers of Aβ and tau pathology and markers of neurodegeneration have been incorporated into a recently proposed biomarker-based "framework" (*58*) The advantage of the modular design of the framework, and considering that reactive gliosis is a critical aspect of the neuropathology of AD, the biomarker framework might to be expanded to include reactive gliosis.

There are several limitations to the study. There is no validation of the semiquantitative or simplified reference region approach by full kinetic analysis with metabolite corrected arterial input function. The same applies to the selection of the reference region. Initial semiquantitative and quantitative examinations used the SWM as reference region. While SWM was affected significantly less by the selegiline regimen than cortical, subcortical or cerebellar regions (~60% vs >85% blockade), the selegiline study clearly indicates that there is substantial specific binding in SWM. This, in principle, would preclude the use of SWM as reference region. It could be argued that SWM represents a brain region that is not likely be involved in the early disease process, although there is SWM atrophy in AD, atrophy is more prevalent around MTL structures (*56*). Another issue to consider is that SWM, *strictu sensu*, does not truly fulfill the criteria for "reference region" (*53*) given it has a completely different cellular composition, it has about half of the regional cerebral blood flow than grey matter, and is likely to have a completely different degree of non-specific binding. It should be more appropriate to call it an internal brain "scaling" region. The kinetic analysis was performed pooling controls and MCI together, where 30% were deemed to have high Aβ. Probably due to the small numbers there were no significant kinetic differences between controls and MCI, nor when comparing Aβ- with Aβ+.

CONCLUSION

Our first-in-human studies confirmed ^{18}F-SMBT-1 is a selective MAO-B tracer. While the main goal was to characterize a MAO-B tracer to be used as surrogate marker of astrogliosis in neurodegenerative conditions, the potential applications of a MAO-B tracer are much wider, extending from neuropsychiatric conditions like depression (*30*) to movement disorders (*59*). In the particular case of assessing astrogliosis, ^{18}F-SMBT-1 will allow a better understanding of the pathophysiology of AD, while examining its potential direct or indirect effect over neurodegeneration, cognitive decline and clinical progression, enabling more accurate staging and prognosis at earlier stages of the disease.

ACKNOWLEDGEMENTS

The study was supported in part by National Health Medical Research Council (NHMRC) of Australia grants G1005121 and grant 19KK0212 from Japan. The funding sources had no input into the design of this study, the analysis of data, or writing of the manuscript.

The authors would like to thank the Brain Research Institute for support in acquiring the MRI data.

The authors would like to thank Dr Chester Mathis, Dr William E Klunk, Dr Milos Ikonomovic, Dr Oscar Lopez, Dr Ann Cohen, Dr Howard Aizenstein, Dr Scott Mason, Dr Beth Snitz and Dr Beth Shaaban at the University of Pittsburgh for extremely fruitful discussions around SMBT-1, MAO-B and reactive astrogliosis.

We thank the participants who took part in the study and their families

KEY POINTS

QUESTION: Is ^{18}F-SMBT-1 a selective MAO-B tracer?

PERTINENT FINDINGS: In a clinical study in 59 elderly and 10 young participants showed that ^{18}F-SMBT-1 is a highly selective MAO-B tracer, with reversible kinetics and low specific signal that follows the known regional distribution of MAO-B in the brain and captures the known MAO-B increases with age.

IMPLICATIONS FOR PATIENT CARE: ^{18}F-SMBT-1 can be used as a surrogate marker of reactive astrogliosis

REFERENCES

1. Masters CL, Beyreuther K. The neuropathology of Alzheimer's disease in the year 2005. In: Beal MF, Lang AE, Ludolph AC, eds. *Neurodegenerative Diseases: Neurobiology, Pathogenesis and Therapeutics*. Cambridge: Cambridge University Press; 2005:433-440.

2. Escartin C, Galea E, Lakatos A, et al. Reactive astrocyte nomenclature, definitions, and future directions. *Nat Neurosci.* 2021;24:312-325.

3. Fakhoury M. Microglia and astrocytes in Alzheimer's disease: Implications for therapy. *Curr Neuropharmacol.* 2018;16:508-518.

4. Vasile F, Dossi E, Rouach N. Human astrocytes: structure and functions in the healthy brain. *Brain Struct Funct.* 2017;222:2017-2029.

5. Adamsky A, Kol A, Kreisel T, et al. Astrocytic activation generates de novo neuronal potentiation and memory enhancement. *Cell.* 2018;174:59-71 e14.

6. Kol A, Adamsky A, Groysman M, Kreisel T, London M, Goshen I. Astrocytes contribute to remote memory formation by modulating hippocampal-cortical communication during learning. *Nat Neurosci.* 2020;23:1229-1239.

7. Osborn LM, Kamphuis W, Wadman WJ, Hol EM. Astrogliosis: An integral player in the pathogenesis of Alzheimer's disease. *Prog Neurobiol.* 2016;144:121-141.

8. Danbolt NC, Furness DN, Zhou Y. Neuronal vs glial glutamate uptake: Resolving the conundrum. *Neurochem Int.* 2016;98:29-45.

9. Carter SF, Herholz K, Rosa-Neto P, Pellerin L, Nordberg A, Zimmer ER. Astrocyte biomarkers in Alzheimer's Disease. *Trends Mol Med.* 2019;25:77-95.

10. Iadecola C, Nedergaard M. Glial regulation of the cerebral microvasculature. *Nat Neurosci.* 2007;10:1369-1376.

11. Koehler RC, Roman RJ, Harder DR. Astrocytes and the regulation of cerebral blood flow. *Trends Neurosci.* 2009;32:160-169.

12. Zhao J, O'Connor T, Vassar R. The contribution of activated astrocytes to Abeta production: implications for Alzheimer's disease pathogenesis. *J Neuroinflammation.* 2011;8:150.

13. Thal DR. The role of astrocytes in amyloid beta-protein toxicity and clearance. *Exp Neurol.* 2012;236:1-5.

14. Perez-Nievas BG, Serrano-Pozo A. Deciphering the astrocyte reaction in Alzheimer's disease. *Front Aging Neurosci.* 2018;10:114.

15. Zamanian JL, Xu L, Foo LC, et al. Genomic analysis of reactive astrogliosis. *J Neurosci.* 2012;32:6391-6410.

16. Liddelow SA, Barres BA. Reactive astrocytes: production, function, and therapeutic potential. *Immunity.* 2017;46:957-967.

17. Sofroniew MV. Astrogliosis. *Cold Spring Harb Perspect Biol.* 2014;7:a020420.

18. Birch AM. The contribution of astrocytes to Alzheimer's disease. *Biochem Soc Trans.* 2014;42:1316-1320.

19. Acioglu C, Li L, Elkabes S. Contribution of astrocytes to neuropathology of neurodegenerative diseases. *Brain Res.* 2021:147291.

20. Ingelsson M, Fukumoto H, Newell KL, et al. Early Abeta accumulation and progressive synaptic loss, gliosis, and tangle formation in AD brain. *Neurology.* 2004;62:925-931.

21. Kreisl WC, Lyoo CH, Liow JS, et al. (11)C-PBR28 binding to translocator protein increases with progression of Alzheimer's disease. *Neurobiol Aging.* 2016;44:53-61.

22. Carter SF, Scholl M, Almkvist O, et al. Evidence for astrocytosis in prodromal Alzheimer disease provided by 11C-deuterium-L-deprenyl: a multitracer PET paradigm combining 11C-Pittsburgh compound B and 18F-FDG. *J Nucl Med.* 2012;53:37-46.

23. Assefa BT, Gebre AK, Altaye BM. Reactive astrocytes as drug target in Alzheimer's disease. *Biomed Res Int.* 2018;2018:4160247.

24. Ekblom J, Jossan SS, Bergstrom M, Oreland L, Walum E, Aquilonius SM. Monoamine oxidase-B in astrocytes. *Glia.* 1993;8:122-132.

25. Rodriguez-Vieitez E, Ni R, Gulyas B, et al. Astrocytosis precedes amyloid plaque deposition in Alzheimer APPswe transgenic mouse brain: a correlative positron emission tomography and in vitro imaging study. *Eur J Nucl Med Mol Imaging.* 2015;42:1119-1132.

26. Rodriguez-Vieitez E, Saint-Aubert L, Carter SF, et al. Diverging longitudinal changes in astrocytosis and amyloid PET in autosomal dominant Alzheimer's disease. *Brain.* 2016;139:922-936.

27. Scholl M, Carter SF, Westman E, et al. Early astrocytosis in autosomal dominant Alzheimer's disease measured in vivo by multi-tracer positron emission tomography. *Sci Rep.* 2015;5:16404.

28. Engler H, Nennesmo I, Kumlien E, et al. Imaging astrocytosis with PET in Creutzfeldt-Jakob disease: case report with histopathological findings. *Int J Clin Exp Med.* 2012;5:201-207.

29. Jevtic II, Lai TH, J ZP, et al. Newly synthesized fluorinated cinnamylpiperazines possessing low in vitro MAO-B binding. *Molecules.* 2020;25:4941.

30. Moriguchi S, Wilson AA, Miler L, et al. Monoamine Oxidase B total distribution volume in the prefrontal cortex of major depressive disorder: An [11C]SL25.1188 Positron Emission Tomography study. *JAMA Psychiatry.* 2019;76:634-641.

31. Saba W, Valette H, Peyronneau MA, et al. [(11)C]SL25.1188, a new reversible radioligand to study the monoamine oxidase type B with PET: preclinical characterisation in nonhuman primate. *Synapse.* 2010;64:61-69.

32. Tyacke RJ, Myers JFM, Venkataraman A, et al. Evaluation of (11)C-BU99008, a PET ligand for the imidazoline2 binding site in human brain. *J Nucl Med.* 2018;59:1597-1602.

33. Venkataraman AV, Keat N, Myers JF, et al. First evaluation of PET-based human biodistribution and radiation dosimetry of (11)C-BU99008, a tracer for imaging the imidazoline2 binding site. *EJNMMI Res.* 2018;8:71.

34. Kumar A, Koistinen NA, Malarte ML, et al. Astroglial tracer BU99008 detects multiple binding sites in Alzheimer's disease brain. *Mol Psychiatry.* 2021. Epub ahead of print. (doi: 10.1038/s41380-021-01101-5)

35. Calsolaro V, Matthews PM, Donat CK, et al. Astrocyte reactivity with late-onset cognitive impairment assessed in vivo using (11)C-BU99008 PET and its relationship with amyloid load. *Mol Psychiatry.* 2021.

36. Harada R, Okamura N, Furumoto S, et al. 18F-THK5351: A novel PET radiotracer for imaging neurofibrillary pathology in Alzheimer disease. *J Nucl Med.* 2016;57:208-214.

37. Ng KP, Pascoal TA, Mathotaarachchi S, et al. Monoamine oxidase B inhibitor, selegiline, reduces 18F-THK5351 uptake in the human brain. *Alzheimers Res Ther.* 2017;9:25.

38. Harada R, Ishiki A, Kai H, et al. Correlations of (18)F-THK5351 PET with postmortem burden of tau and astrogliosis in Alzheimer disease. *J Nucl Med.* 2018;59:671-674.

39. Harada R, Hayakawa Y, Ezura M, et al. (18)F-SMBT-1: A selective and reversible PET tracer for Monoamine Oxidase-B imaging. *J Nucl Med.* 2021;62:253-258.

40. Battle MR, Pillay LC, Lowe VJ, et al. Centiloid scaling for quantification of brain amyloid with [(18)F]flutemetamol using multiple processing methods. *EJNMMI Res.* 2018;8:107.

41. Rowe CC, Jones G, Dore V, et al. Standardized expression of 18F-NAV4694 and 11C-PiB beta-amyloid PET results with the Centiloid scale. *J Nucl Med.* 2016;57:1233-1237.

42. Navitsky M, Joshi AD, Kennedy I, et al. Standardization of amyloid quantitation with florbetapir standardized uptake value ratios to the Centiloid scale. *Alzheimers Dement.* 2018;14:1565-1571.

43. Klunk WE, Koeppe RA, Price JC, et al. The Centiloid Project: standardizing quantitative amyloid plaque estimation by PET. *Alzheimers Dement.* 2015;11:1-15 e11-14.

44. Bourgeat P, Dore V, Fripp J, et al. Implementing the Centiloid transformation for (11)C-PiB and beta-amyloid (18)F-PET tracers using CapAIBL. *Neuroimage.* 2018;183:387-393.

45. Krishnadas N, Dore V, Lamb F, et al. Case report: (18)F-MK6240 tau Positron Emission Tomography pattern resembling Chronic Traumatic Encephalopathy in a retired Australian Rules Football player. *Front Neurol.* 2020;11:598980.

46. Ishiki A, Harada R, Okamura N, et al. Tau imaging with [(18) F]THK-5351 in progressive supranuclear palsy. *Eur J Neurol.* 2017;24:130-136.

47. Jack CR, Jr., Wiste HJ, Weigand SD, et al. Defining imaging biomarker cut points for brain aging and Alzheimer's disease. *Alzheimers Dement.* 2017;13:205-216.

48. Jack CR, Jr., Wiste HJ, Schwarz CG, et al. Longitudinal tau PET in ageing and Alzheimer's disease. *Brain.* 2018;141:1517-1528.

49. Gulyas B, Pavlova E, Kasa P, et al. Activated MAO-B in the brain of Alzheimer patients, demonstrated by [11C]-L-deprenyl using whole hemisphere autoradiography. *Neurochem Int.* 2011;58:60-68.

50. Galva MD, Bondiolotti GP, Olasmaa M, Picotti GB. Effect of aging on lazabemide binding, monoamine oxidase activity and monoamine metabolites in human frontal cortex. *J Neural Transm Gen Sect.* 1995;101:83-94.

51. Fleisher AS, Joshi AD, Sundell KL, et al. Use of white matter reference regions for detection of change in florbetapir positron emission tomography from completed phase 3 solanezumab trials. *Alzheimers Dement.* 2017;13:1117-1124.

52. Chen K, Roontiva A, Thiyyagura P, et al. Improved power for characterizing longitudinal amyloid-beta PET changes and evaluating amyloid-modifying treatments with a cerebral white matter reference region. *J Nucl Med.* 2015;56:560-566.

53. Lammertsma AA, Hume SP. Simplified reference tissue model for PET receptor studies. *Neuroimage.* 1996;4:153-158.

54. Logan J, Fowler JS, Volkow ND, Wang GJ, Ding YS, Alexoff DL. Distribution volume ratios without blood sampling from graphical analysis of PET data. *J Cereb Blood Flow Metab.* 1996;16:834-840.

55. Ichise M, Ballinger JR, Golan H, et al. Noninvasive quantification of dopamine D2 receptors with iodine-123-IBF SPECT. *J Nucl Med.* 1996;37:513-520.

56. Li J, Pan P, Huang R, Shang H. A meta-analysis of voxel-based morphometry studies of white matter volume alterations in Alzheimer's disease. *Neurosci Biobehav Rev.* 2012;36:757-763.

57. Hammond TR, Marsh SE, Stevens B. Immune signaling in neurodegeneration. *Immunity.* 2019;50:955-974.

58. Jack CR, Jr., Bennett DA, Blennow K, et al. A/T/N: An unbiased descriptive classification scheme for Alzheimer disease biomarkers. *Neurology.* 2016;87:539-547.

59. Cohen G, Farooqui R, Kesler N. Parkinson disease: a new link between monoamine oxidase and mitochondrial electron flow. *Proc Natl Acad Sci U S A.* 1997;94:4890-4894.

60. Fowler JS, Volkow ND, Wang GJ, et al. Age-related increases in brain monoamine oxidase B in living healthy human subjects. *Neurobiol Aging.* 1997;18:431-435.

FIGURE LEGENDS

Figure 1. Effect of Selegiline on ^{18}F-THK5351 and ^{18}F-SMBT-1

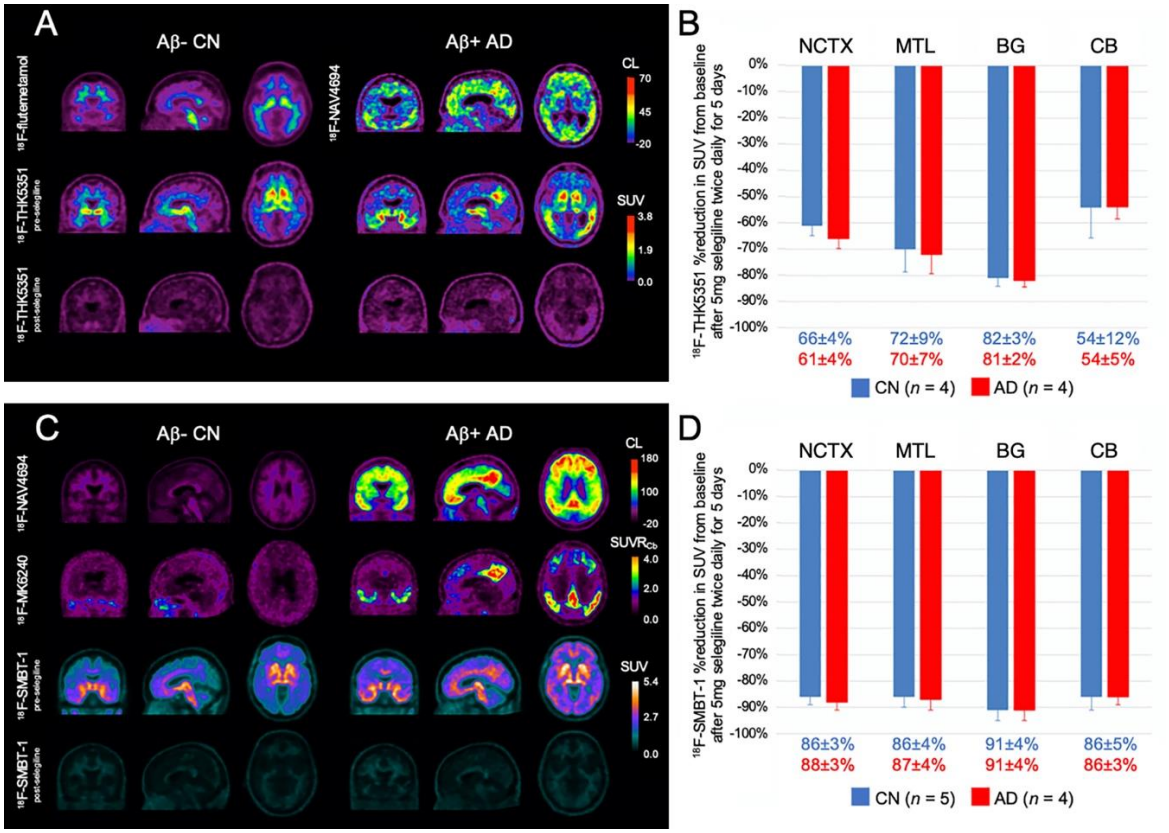

A. Representative coronal, sagittal and transaxial PET images in an Aβ- cognitively unimpaired control (CN, 79 yo M, MMSE 29) and in an Aβ+ Alzheimer's disease (AD) patient (72 yo M, MMSE 24). Aβ imaging studies expressed in Centiloids (CL, top row) performed with ^{18}F-flutemetamol or ^{18}F-NAV4694-. Baseline ^{18}F-THK5351 PET images (middle row) of the same individuals before and after (bottom row) the selegiline regimen indicating a variable degree of regional blockade of ^{18}F-THK5351, most noticeable in basal ganglia (BG), mesial temporal lobe (MTL) and neocortex (NCTX). Given that there is significant reduction in tracer retention in the cerebellar cortex, all images are displayed in Standard Uptake Value (SUV) units. While in the controls participants there is significant reduction of ^{18}F-THK5351 retention throughout the brain, in the AD patients there is residual cortical retention likely due to ^{18}F-THK5351 binding to tau.

B. Bar graphs showing %degree of selegiline ^{18}F-THK5351 regional blockade in neocortex (NCTX, ~63% decrease), mesial temporal lobe (MTL, ~71% decrease), basal ganglia (BG, ~82% decrease) and cerebellar cortex (CB, ~54% decrease). Reduction of the signal was greater in BG

and MTL than in NCTX and CB, although there were no significant differences in the degree of signal reduction between controls and AD

C. Representative coronal, sagittal and transaxial PET images in an Aβ-T- cognitively unimpaired control (CN, 78 yo F, MMSE 29) and in an Aβ+T+ Alzheimer's disease (AD) patient (75 yo F, MMSE 21). Aβ imaging studies performed with ^{18}F-NAV4694 are expressed in Centiloids (CL, top row). Second row shows tau imaging studies expressed in SUVR using the cerebellar cortex as reference region, performed with either ^{18}F-MK6240 or ^{18}F-PI2620. Baseline ^{18}F-SMBT-1 PET images (third row) of the same individuals before and after (bottom row) the selegiline regimen indicating a high degree of regional blockade of ^{18}F-SMBT-1, across all regions of the brain. As with the ^{18}F-THK5351 studies, all ^{18}F-SMBT-1 PET images are displayed in Standard Uptake Value (SUV) units. In contrast with was observed with ^{18}F-THK5351 (Fig 1A), there was no residual cortical retention in the controls or AD patients.

D. Bar graphs showing a high %degree of blocking of ^{18}F-SMBT-1 by selegiline, with >85% blockade across all regions of the brain, indicating selective binding of ^{18}F-SMBT-1 to MAO-B as well as low non-specific binding. There were no significant differences in the degree of signal reduction between regions nor between controls and AD.

Abbreviations: CN (age-matched control); AD (Alzheimer's disease); SUV (Standard Uptake Value); SUVR (Standard Uptake Value Ratio); NCTX (neocortex); MTL (mesial temporal lobe); BG (basal ganglia); CB (cerebellar cortex).

Figure 2. Regional Brain Distribution of MAO-B in the brain: Correlation between in vitro autoradiography with ^{11}C-DED and ^{18}F-SMBT-1 retention in Aβ- elderly controls

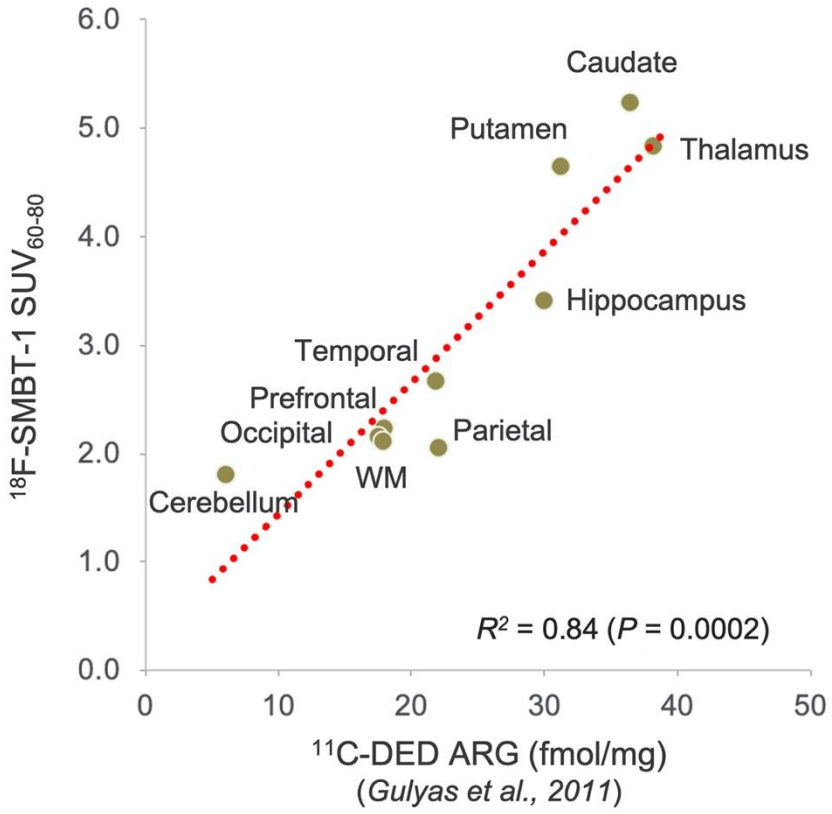

There was a high correlation (R^2=0.84) between the known in vitro regional distribution of MAO-B in the brain (*49*), expressed in fmol/mg, and the regional SMBT-1 retention at 60-80 min post injection.

Abbreviations: SUV (Standard Uptake Value); ARG (autoradiography)

Figure 3. Effect of Age

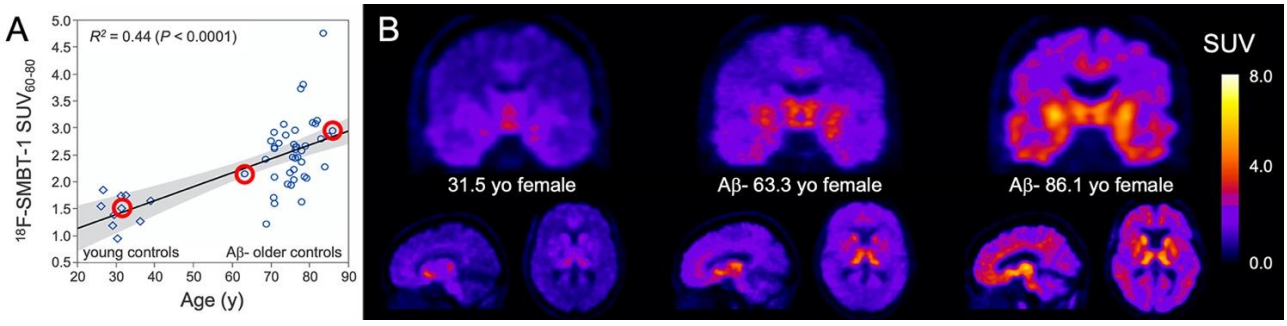

A. ^{18}F-SMBT-1 SUV$_{60-80}$ in the frontal lobe of 10 young controls (5F/5M, 31.3±4.0 yo) and 44 Aβ- elderly controls (25F/19M, 76.0±4.8 yo) was able to capture the reported age-related increases of MAO-B in the frontal lobe as previously reported by in vitro studies (*50*) and in vivo with PET (*60*).

B. Coronal, sagittal and transaxial ^{18}F-SMBT-1 images illustrating the age-related regional increases in ^{18}F-SMBT-1 signal in three females whose ages ranged from 31 to 86 yo. (identified by the red circles on Figure 4A).

Abbreviations: SUV, (Standard Uptake Value); Aβ-, low Aβ.

Figure 4. ^{18}F- SMBT-1: Time-activity and total binding curves

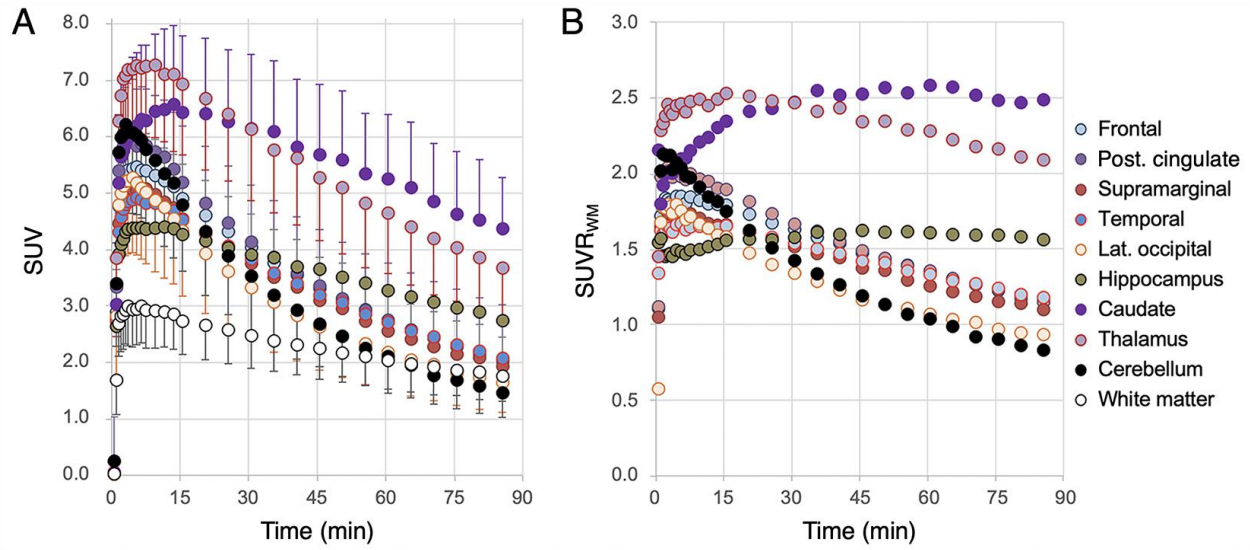

A. Time activity curves reveal ^{18}F-SMBT-1 has robust entry into the brain (SUV=5-7 at ~5 min after injection) and displays reversible kinetics. ^{18}F-SMBT-1 clearance was slower in areas of high concentrations of MAO-B such as the basal ganglia and the hippocampus, and faster in regions with lower MAO-B concentrations such as frontal, temporal and cerebellum.

B. Tissue ratios -using the subcortical white matter (SWM) as reference region- over time shows $SUVR_{SWM}$ approaching apparent steady state in high binding areas ~50 min after injection. The SWM was found to be the more stable reference region across clinical groups and across Aβ status.

Abbreviations: SUV (Standard Uptake Value); SUVR (Standard Uptake Value Ratio)

Graphical abstract

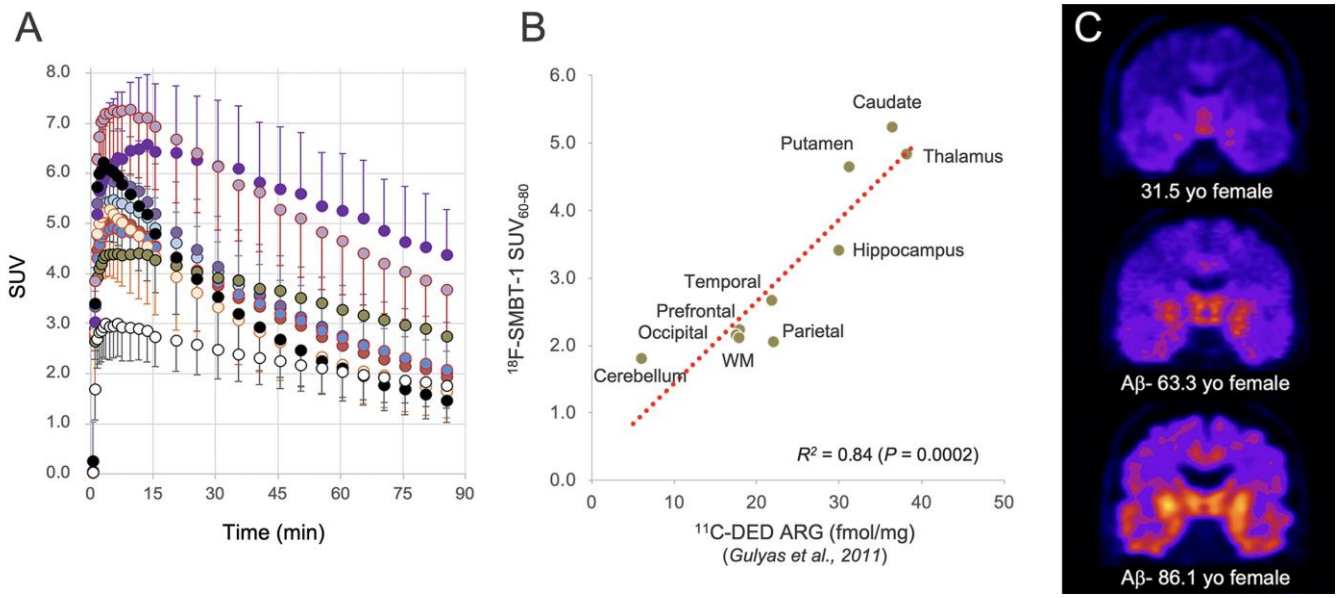

Table 1. Demographics of the ^{18}F-THK5351 and ^{18}F-SMBT-1 selectivity evaluations

	THK5351 CN	THK5351 AD/MCI	SMBT-1 CN	SMBT-1 AD
n	4	4	5	4
Age (years)	79.1±6.7	74.9±7.0	78.5±6.0	76.7±1.5
Sex	3M/1F	2M/2F	2M/3F	1M/3F
%APOE4	25%	50%	60%	67%
MMSE	29.3±0.5	25.7±2.8*	29.2±0.8	22.8±4.8*
CDR SoB	0.0±0.0	2.2±0.4*	0.0±0.0	7.6±2.1*
Aβ (CL)	28.3±54.7	82.7±12.7	17.4±10.2	127.6±47.1
%Aβ+	25%	100%	60%	100%

Abbreviations: CN: age-matched controls; MCI: mild cognitive impairment; AD: Alzheimer's disease; CL: Centiloids, MMSE: Mini Mental State Examination; CDR-SoB: Clinical Dementia Rating-Sum of Boxes.

**Significantly different ($p<0.05$)*

Table 2. Percentage reduction in regional ^{18}F-THK5351 and ^{18}F-SMBT-1 SUV by selegiline

REGION	^{18}F-THK-5351		CN≠AD		^{18}F-SMBT-1		CN≠AD
	CN	AD	*p*		CN	AD	*p*
Caudate	-86%	-84%	*n.s.*		93%	95%	*n.s.*
Thalamus	-83%	-82%	*n.s.*		93%	95%	*n.s.*
Putamen	-80%	-78%	*n.s.*		92%	92%	*n.s.*
Anterior Cingulate	-76%	-74%	*n.s.*		88%	90%	*n.s.*
Hippocampus	-69%	-64%	*n.s.*		88%	90%	*n.s.*
Frontal Cortex	-67%	-63%	*n.s.*		87%	89%	*n.s.*
Temporal	-67%	-67%	*n.s.*		87%	88%	*n.s.*
Posterior Cingulate	-66%	-63%	*n.s.*		86%	88%	*n.s.*
Parietal	-63%	-56%	*n.s.*		85%	86%	*n.s.*
Cerebellar Cortex	-54%	-54%	*n.s.*		86%	86%	*n.s.*
Whole Cerebellum	-72%	-68%	*n.s.*		83%	83%	*n.s.*
Pons	-73%	-68%	*n.s.*		82%	82%	*n.s.*
Midbrain	-66%	-63%	*n.s.*		82%	81%	*n.s.*
Occipital	-61%	-56%	*n.s.*		80%	83%	*n.s.*
Cerebellar WM	-65%	-56%	*n.s.*		69%	69%	*n.s.*
SWM+CC	-64%	-57%	*n.s.*		62%	65%	*n.s.*
SWM	-54%	-54%	*n.s.*		60%	63%	*n.s.*

Abbreviations: CN, age-matched controls, AD: Alzheimer's disease; WM: white matter: SWM: subcortical white matter; Cb: cerebellum; CC: corpus callosum

Table 3 Demographics for the assessment of the effect of age

	YOUNG CONTROLS	ELDERLY Aβ- CONTROLS
n	10	44
Age (years)	31.3±4.0*	76.0±4.8
Sex (%females)	50%	57%
Education (years)		14.8±2.7
%APOE4		30%
MMSE		28.6±1.5
CDR SoB		0.07±0.2
Aβ burden (CL)		0.80±6.9

Abbreviations: CL: Centiloids, MMSE: Mini Mental State Examination; CDR-SoB: Clinical Dementia Rating-Sum of Boxes.

**Significantly different ($p<0.05$)*

Table 4. Demographics for assessing ^{18}F-SMBT-1 tracer kinetics

	CN/MCI
n	10
Age (years)	73.2±7.2
Gender (%females)	30%
%APOE4	60%
MMSE	27.7±1.6
CDR SoB	0.3±0.4
Aβ burden (CL)	15.8±31.0
%Aβ+	30%

Abbreviations: CL: Centiloids, MMSE: Mini Mental State Examination; CDR-SoB: Clinical Dementia Rating-Sum of Boxes.

Table 5. Correlation between MAO-B in vitro distribution and ^{18}F-SMBT-1 binding parameters and tissue ratios generated with different reference regions

	r	95% CI	*p*
$SUVR_{SWM}$	0.914	0.62-0.98	0.0002
$SUVR_{Cb}$	0.904	0.61-0.98	0.0007
$SUVR_{SWM+CC}$	0.889	0.55-0.98	0.0013
$SUVR_{CbWM}$	0.888	0.55-0.98	0.0014
Ichise BP_{ND}	0.885	0.54-0.98	0.0015
Logan DVR	0.849	0.42-0.97	0.0038

Correlation between in vitro MAO-B brain distribution assessed with autoradiography (*49*) and quantitative and semiquantitative measures of SMBT-1 binding, ranked by correlation coefficients (*r*). Tissue ratios and graphical analysis results using the subcortical white matter (SWM) as reference region yielded the highest correlation with in vitro measures of MAO-B.

Abbreviations: SUVR: Standard Uptake Value Ratio, BPND: Binding Potential Non-Displaceable; DVR: Total Distribution Volume Ratio; WM: white matter: SWM: subcortical white matter; Cb: cerebellum; CC: corpus callosum

SUPPLEMENTARY MATERIALS

^{18}F-SMBT-1 synthesis

[^{18}F]Fluoride was produced in the cyclotron by ^{18}O(p, n) ^{18}F reaction on enriched [^{18}O]H_2O. The resulting [^{18}F]Fluoride was activated with Kryptofix 222 and then reacted the tosylate precursor (2.5 mg/1 mL dimethylsulfoxide). The solution was heated to 110°C for 10min followed by deprotection of the hydroxyl group with hydrochloric acid (0.5 mL 1N, 100°C, 3min). The crude reaction was neutralized with potassium acetate solution and diluted with water for injection (WFI) prior to passing through a Sep-Pak tC18 Plus cartridge (Waters). After rinsing the Sep Pak with WFI the radioactive products were eluted off the cartridge with acetonitrile and diluted with WFI before injection onto a semi preparative HPLC column (Inertsil® ODS-3 5µM, 10 X 250mm (GL Sciences, Inc., Tokyo, Japan); mobile phase: 20 mmol/L NaH_2PO_4/acetonitrile (67/33); flow rate: 5.0 mL/min). Purified ^{18}F-SMBT-1 was reformulated for injection using a Sep-Pak tC18 Plus cartridge. The final product contained ^{18}F-SMBT-1, <10% Ethanol, sodium ascorbate (0.05% v/v) and 0.9% sodium chloride. ^{18}F-SMBT-1 yielded a greater than 95% radiochemical purity after HPLC purification. The average of decay-corrected radiochemical yield was 40% and the molar activity at the end of ^{18}F-SMBT-1 synthesis was >400 GBq/µmol.